Hindawi
Journal of Nanomaterials
Volume 2018, Article ID 8124920, 9 pages
https://doi.org/10.1155/2018/8124920

Research Article

Room-Temperature Preparation of Cobalt-Based Electrocatalysts through Simple Solution Treatment for Selectively High-Efficiency Hydrogen Evolution Reaction in Alkaline or Acidic Medium

Zheng Chen,[1,2] Wenjun Luo,[3] Feng Du,[1,2] Ruyi Wang,[1,2] Liang Li,[1,2] Yong Zhou,[2,3,4] and Zhigang Zou[1,2]

[1]*National Laboratory of Solid State Microstructures, Collaborative Innovation Center of Advanced Microstructures, Department of Physics, Nanjing University, Nanjing 210093, China*
[2]*Eco-materials and Renewable Energy Research Center (ERERC), Nanjing University, Nanjing 210093, China*
[3]*Key Laboratory of Flexible Electronics (KLOFE) & Institute of Advanced Materials (IAM), Jiangsu National Synergetic Innovation Center for Advanced Materials (SICAM), Nanjing Tech University (NanjingTech), 30 South Puzhu Road, Nanjing 211816, China*
[4]*Key Laboratory of Modern Acoustics, MOE, Institute of Acoustics, Department of Physics, Nanjing University, Nanjing 210093, China*

Correspondence should be addressed to Yong Zhou; zhouyong1999@nju.edu.cn

Received 4 May 2018; Revised 13 August 2018; Accepted 15 August 2018; Published 6 September 2018

Academic Editor: Xuping Sun

The versatile cobalt-phosphorus (Co-P) precursor was synthesized on Ni foam (NF) with an electrodeposition method. Simple room-temperature treatment of the precursor with 1 M NaOH and 0.5 M H_2SO_4 allows for the production of cobalt oxide nanorods (Co_xO_y/NF) and cobalt phosphate/phosphide (Co-Pi/CoP/NF), respectively. The resulting Co_xO_y/NF shows a low overpotential (η_{10}) of 80 mV at −10 mA/cm^2 in an alkaline electrolyte (pH = 14) for a hydrogen evolution reaction (HER) toward electrocatalytic water splitting. The Co-Pi/CoP/NF exhibits a low η_{10} of 112 mV in an acidic electrolyte (pH = 0), in which the synergy between Co (+2) and Co (+3) may play an important role in the reaction.

1. Introduction

Hydrogen is widely considered as a clean and renewable fuel which is a promising replacement for fossil fuels [1–3]. Electrochemical and photoelectrochemical processes for water splitting are favourable strategies benefiting from abundant water resources and giving high-purity H_2 production [4–7]. Overall, water splitting involves two half reactions: hydrogen evolution reaction (HER) and oxygen evolution reaction (OER). The mechanism of the HER process in an alkaline electrolyte can be considered as a combination of the following three basic steps: (1) the electroreduction of water molecules and absorption of hydrogen (Volmer reaction): $M + H_2O + e^- \rightarrow M - H_{ads} + OH^-$, (2) electrochemical hydrogen absorption (Heyrovsky reaction): $M - H_{ads} + H_2O + e^- \rightarrow M + H_2 + OH^-$, and (3) chemical desorption (Tafel reaction): $2M - H_{ads} \rightarrow 2M + H_2$. Similarly, the process in an acidic electrolyte can be regarded as the following three basic steps: (1) the electroreduction of water molecules and absorption of hydrogen (Volmer reaction): $M + H_3O^+ + e^- \rightarrow M - H_{ads} + H_2O$, (2) electrochemical hydrogen absorption (Heyrovsky reaction): $M - H_{ads} + H_3O^+ + e^- \rightarrow M + H_2 + H_2O$, and (3) chemical desorption (Tafel reaction): $2M - H_{ads} \rightarrow 2M + H_2$, where M represents a metal atom and H_{ads} stands for a H atom absorbed at an active site of the catalyst [8–13].

To achieve sustainable production of H_2 fuel through water splitting, much effort has been made to design highly efficient electrocatalysts that are vital for lowering the dynamic overpotential during the HER. Currently, Pt is the most efficient catalyst for HER [14, 15]. However, the low natural abundance and high cost of Pt greatly limit their application in large-scale commercial production. Therefore, the synthesis of noble metal-free electrocatalysts with high efficiency for HER has drawn much attention. Over the past few years, researchers report various kinds of electrocatalysts such as metal chalcogenides [16, 17], metal carbides [14, 18], metal nitrides [19, 20], metal phosphides [21, 22], metal oxide hydroxides [23, 24], and metal alloys [25] with different morphologies and microstructures for HER. Transition metal phosphides and phosphate have drawn intense attention recently because of their remarkable catalytic activity for HER [26–28]. However, there are few noble metal-free electrocatalysts with excellent activity and stability in both acidic and alkaline media [29].

In this study, we report the room-temperature fabrication of Co-based electrocatalysts with excellent catalytic activity and stability in both alkaline and acidic electrolytes through simply treating a Co-P precursor with either an alkaline or acidic solution. The related Co-P precursor was synthesized on Ni foam (NF) with an electrodeposition method. After treatment in an alkaline and acidic solution, Co_xO_y/NF and Co-Pi/CoP/NF electrodes were obtained, respectively. The resulting Co_xO_y/NF electrode shows a low η_{10} of 80 mV for HER in an alkaline medium, and the Co-Pi/CoP/NF electrode exhibits a η_{10} of 112 mV in an acidic medium for HER.

2. Experimental Section

2.1. Chemicals and Reagents. Sodium hypophosphite monohydrate ($NaH_2PO_2{\cdot}H_2O$), cobaltous chloride hexahydrate ($CoCl_2{\cdot}6H_2O$), sodium chloride (NaCl), boric acid (H_3BO_3), ethanol (CH_3CH_2OH), sodium hydroxide (NaOH), hydrochloric acid (HCl, 36–38 wt%), and sulfuric acid (H_2SO_4, 98 wt%) were all purchased from Alfa Aesar with an analytical reagent (AR) and were used without further purification.

2.2. Sample Preparation. The Co-P precursor electrodeposited on a Ni foam was prepared by galvanostatic electrodeposition in a standard three-electrode system. A platinum (Pt) sheet, a silver chloride electrode (Ag/AgCl, saturated potassium chloride solution), and a piece of Ni foam were used as the counter, reference, and working electrode, respectively. Before electrodeposition, the Ni foam was cleaned with deionized water and ethanol in an ultrasonic cleaner for 10 minutes each to remove the contaminants on its surface. Then, it was ultrasonically cleaned with 1 M HCl for about 10 minutes to get rid of the oxide. After that, the Ni foam was washed with deionized water and dried for further use. The electrolyte in the electroplating bath consists of 0.3 M $NaH_2PO_2{\cdot}H_2O$, 0.2 M $CoCl_2{\cdot}6H_2O$, 0.15 M H_3BO_3, and 0.1 M NaCl. The electrodeposition was carried out at a potential of −1.5 V vs. a Ag/AgCl reference electrode for 10 minutes. To get Co_xO_y/NF (Co_xO_y on Ni foam) and Co-Pi/CoP/NF (Co-Pi/CoP thin film on Ni foam) electrodes, the as-prepared Co-P precursor was washed with deionized water and subsequently immersed in 1 M NaOH (pH = 14) or 0.5 M H_2SO_4 (pH = 0) for 12 hours at room temperature.

2.3. Characterization. The morphologies of the synthesized samples were recorded by scanning electron microscopy (SEM, S-3400N II, Hitachi Co., Japan) with an acceleration voltage of 20 kV. Transmission electron microscopy (TEM) images, high-resolution transmission electron microscopy (HRTEM) images, electron diffraction pattern, and element-mapping images were obtained on a JEOL JEM-2100 microscope with a LaB_6 filament and an accelerating voltage of 200 kV. XPS was measured on a PHI 5000 VersaProbe X-ray photoelectron spectroscope (ULVAC-PHI Inc., Japan).

2.4. Electrochemical Measurements. All catalytic performances were conducted on a CHI660E electrochemical analyzer/workstation (Chenhua Instruments, Shanghai) using a typical three-electrode system at room temperature. The as-prepared electrodes (Co_xO_y/NF, Co-Pi/CoP/NF), Ni foam, and Pt sheet were used as the working electrodes. The Pt sheet and Ag/AgCl electrode were used as the counter and reference electrode, respectively. Linear sweep voltammetry (LSV) and Tafel plot were conducted, and LSV was carried out at a scan rate of 2 mV/s. For HER in alkaline and acidic media, 1 M NaOH (pH = 14) and 0.5 M H_2SO_4 (pH = 0) were used as the electrolyte. During these tests, the working surface area of the as-prepared samples was adjusted by changing the length of the Ni foam immersed in the electrolyte and the area was estimated to be 1 cm^2. All the overpotentials measured in this work were calibrated with the reversible hydrogen electrode (RHE) according to

$$E_{\mathrm{RHE}} = E_{\mathrm{Ag/AgCl}} + 0.197 + 0.0591 \times \mathrm{pH}. \quad (1)$$

3. Results and Discussion

The Co-P precursor was synthesized with a typical three-electrode system by electrodeposition. $NaH_2PO_2{\cdot}H_2O$ and $CoCl_2{\cdot}6H_2O$ serve as the source of the P and Co atoms. The precursor was then immersed in 1 M NaOH or 0.5 M H_2SO_4 to obtain the Co_xO_y/NF and Co-Pi/CoP/NF electrodes, respectively. Figure 1 shows the morphology of the Co-P precursor and those of Co-Pi/CoP/NF and Co_xO_y/NF. The surface of the Ni foam was covered by a solid sphere-like Co-P precursor after the completion of electrodeposition. Co-Pi/CoP/NF exhibits a thin-film morphology and Co_xO_y/NF consists of lots of nanorods. Figures 2(a)–2(c) present the TEM images of the as-synthesized products. The Co-P precursor shows an irregular microstructure. The Co-Pi/CoP features large amounts of interlacing thin wires, which can explain the film structure presented in the SEM image in Figure 1. Since the catalysts seem to be amorphous, the characteristic peaks of our catalysts can hardly be found in the XRD pattern, especially for Co-Pi. A similar situation has been reported earlier [30, 31].

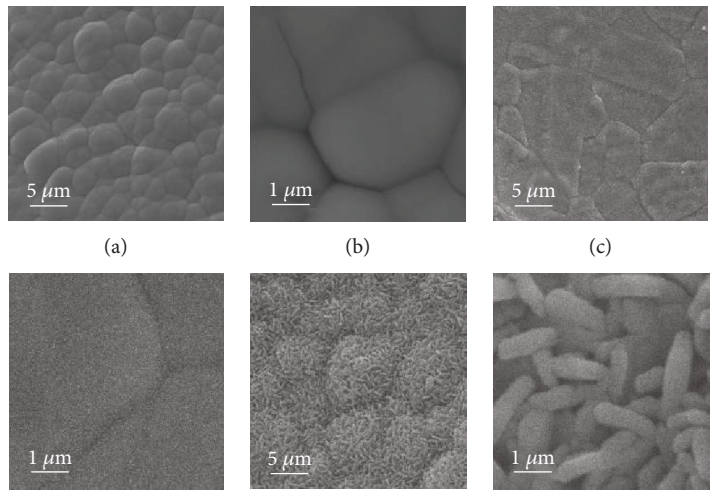

Figure 1: SEM images of (a-b) the Co-P precursor, (c-d) Co-Pi/CoP electrode, and (e-f) Co_xO_y electrode.

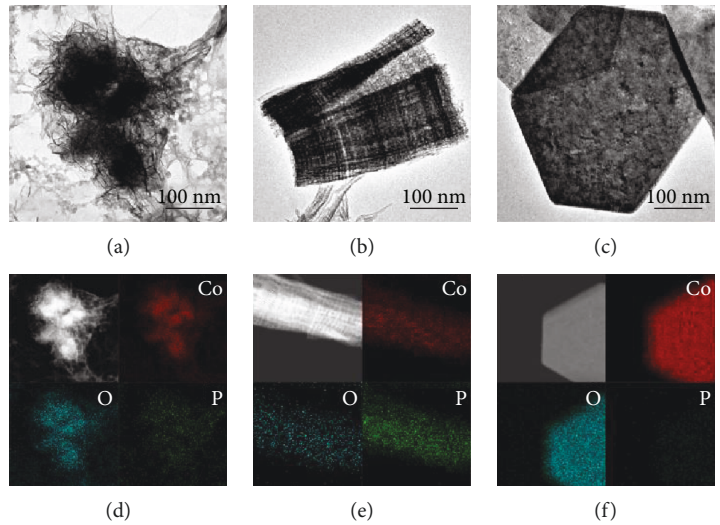

Figure 2: TEM images of (a) the Co-P precursor, (b) Co-Pi/CoP catalyst, and (c) Co_xO_y catalyst. Element mapping images of Co, O, and P in (d) the Co-P precursor, (e) Co-Pi/CoP catalyst, and (f) Co_xO_y catalyst.

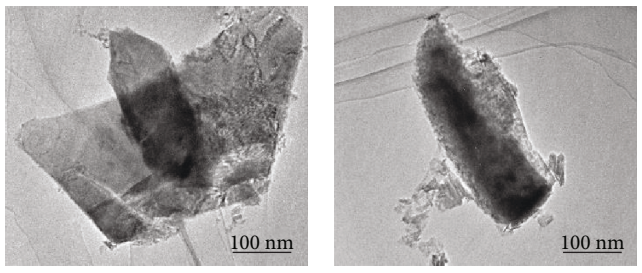

Figure 3: TEM images of the Co_xO_y catalyst with a different structure.

Table 1: Atom concentration of Co, O, and P in the Co-P precursor and in Co-Pi/CoP and Co_xO_y.

	C	Co	P	O
Co-P precursor	47.46	9.87	9.92	32.75
Co-Pi/CoP	48.26	11.08	16.89	23.77
Co_xO_y	46.54	10.33	1.04	42.09

For Co_xO_y, the existence of oxides in different valence states makes its morphology not single. Figure 2(c) presents the structure of a hexagonal nanoplate, and Figure 3 shows the nanorod structure which is consistent with the nanorods observed in the SEM images. We can also find the nanoplate structure although the nanoplate structure seems to be broken. Figures 2(d)–2(f) show the element mapping, from which the existence of Co, O, and P can be easily detected in all products.

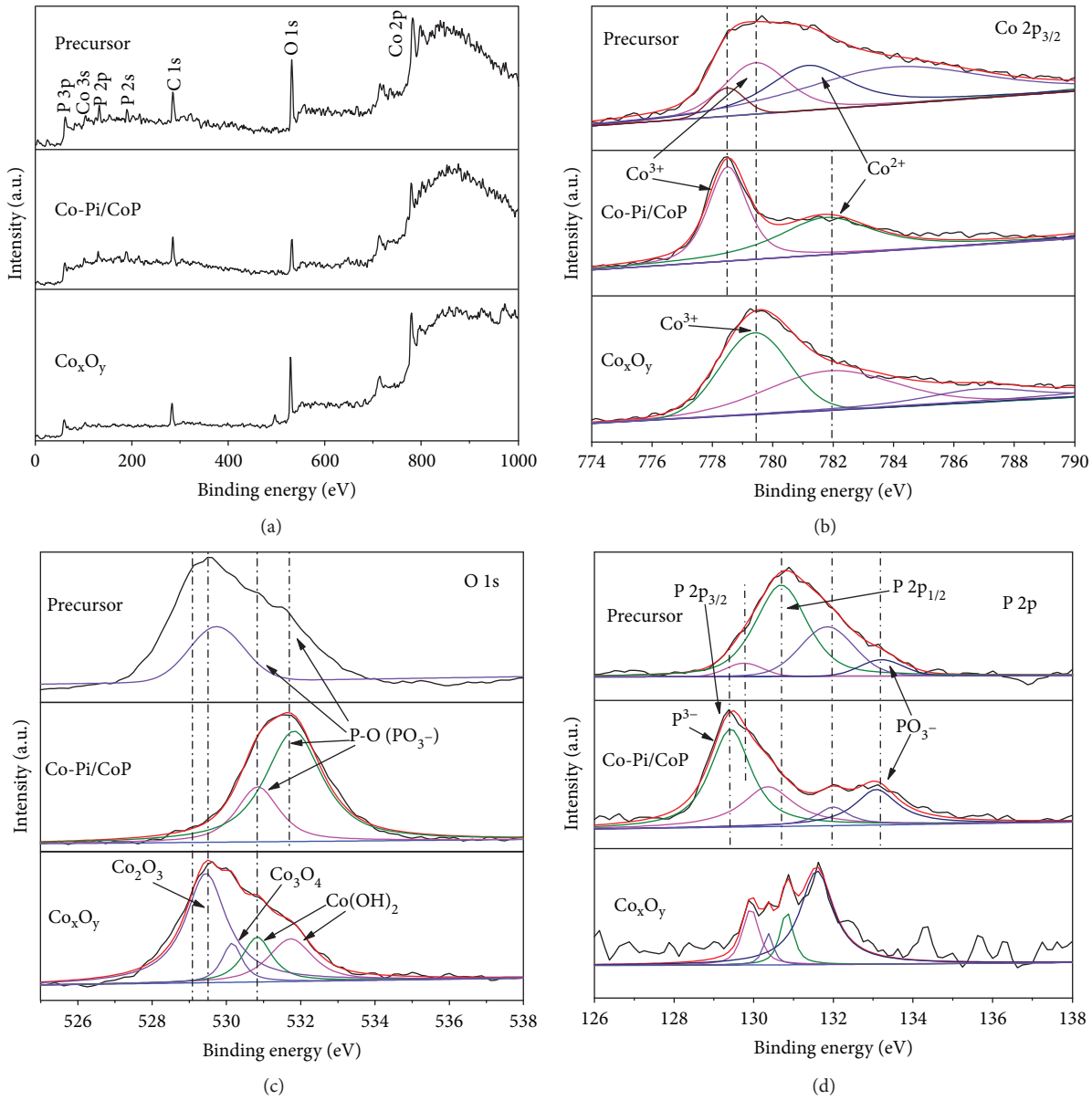

FIGURE 4: (a) The total XPS survey spectra for the Co-P precursor and Co-Pi/CoP/NF and Co_xO_y/NF electrodes; XPS spectrum of (b) the $Co_{2p3/2}$ region, (c) O_{1s} region, and (d) P_{2p} region for the Co-P precursor and Co-Pi/CoP/NF and Co_xO_y/NF electrodes.

XPS spectra further confirm the atom ratio, element composition, and chemical bonding of as-synthesized samples. Table 1 shows that the atom concentration makes a difference to the original precursor after treatment with an acidic or alkaline solution. It reveals that the atom ratio of Co : P is about 1 : 1, 2 : 3, and 10 : 1 in the Co-P precursor, Co-Pi/CoP, and Co_xO_y respectively. It is noteworthy that P can hardly be found after being treated with an alkaline solution. It means that the P moiety was rinsed from the Ni foam. Figure 4(a) shows the total XPS survey spectra for the Co-P precursor and the Co_xO_y and Co-Pi/CoP electrocatalysts. It is consistent with element mapping that three elements (Co, O, and P) exist, and no obvious peaks for other elements are observed. Furthermore, the high-resolution XPS spectra for $Co_{2p3/2}$, O_{1s}, and P_{2p} are presented in Figures 4(b)–4(d). The binding energy of Co_{2p} appears in two peaks around 780 eV and 796 eV which are ascribed to $Co_{2p3/2}$ and $Co_{2p1/2}$ with their satellites beside them, respectively. The peaks for $Co_{2p3/2}$ show that Co exists not only in the +2 but also in the +3 state. The representative peaks for Co^{2+} locate at 781.2 eV and 781.9 eV, and the peaks for Co^{3+} locate at 778.4 eV [32, 33]. The presence of Co^{3+} indicates the potential existence of CoP. The peak between 129.3 eV and 129.6 eV corresponding to P^{3-} exactly confirms the presence of CoP [26, 33, 34]. Furthermore, the binding energy of 131.9 eV and 133.2 eV corresponds to phosphate, which suggests the existence of Co-Pi [29]. For the O_{1s} spectra, the peaks appearing at 530.9 eV and 531.8 eV can be assigned to the P-O bonding, which also confirms

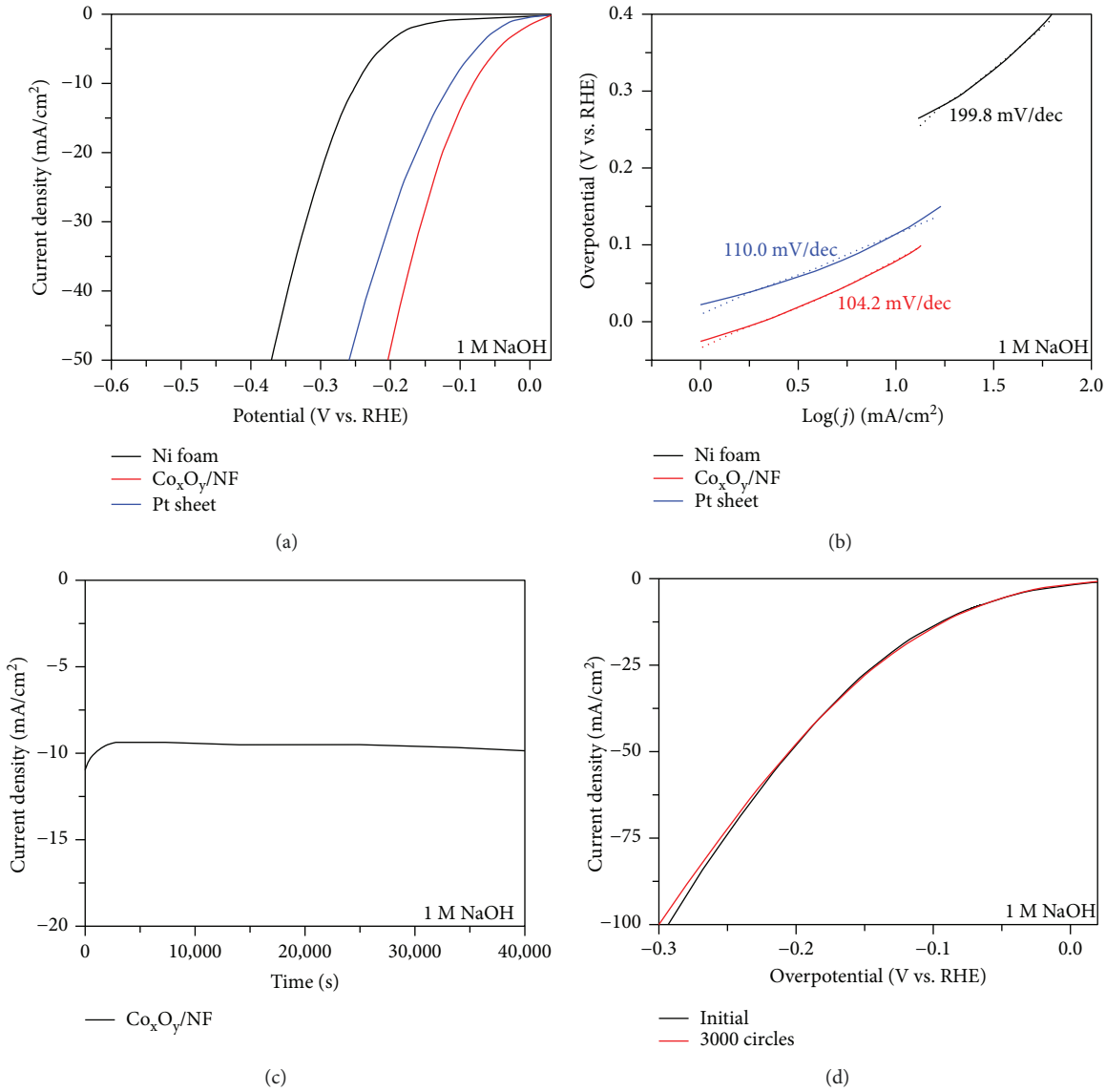

Figure 5: (a) LSV polarization curves for HER and (b) the corresponding Tafel slopes of bare Ni foam, Co_xO_y/NF, and Pt sheet in 1 M NaOH (pH = 14). (c) Chronoamperometry curves of the long-term stability of the Co_xO_y/NF electrode at a static overpotential of 80 mV in 1 M NaOH. (d) Polarization curves obtained over Co_xO_y/NF before and after potential sweeps between −0.2 and +0.2 V vs. RHE for 3000 cycles with a scan rate of 0.1 V/s.

the existence of Co-Pi [26, 29]. The binding energy between 529.0 eV and 529.5 eV is related to the Co-O bonding [33, 35], which may be caused by oxidation in air. The peak located at 530.8 eV and 531.5 eV can be attributed to $Co(OH)_2$ [36, 37]. In addition, when the precursor is treated with 0.5 M H_2SO_4, obvious bubbles were found on the surface. It is reasonable to believe that Co^{2+} is reduced into Co metal during the electrodeposition process.

Co_xO_y and Co-Pi/CoP electrocatalysts with a unique composition were used as free-standing electrodes for electrocatalytic HER in 1 M NaOH and 0.5 M H_2SO_4. The linear sweep voltammetry (LSV) curves, corresponding Tafel slopes, and chronoamperometry I-t curves were measured on Co_xO_y/NF and Co-Pi/CoP/NF to estimate their HER activity and long-term stability. Control experiments were also performed on a bare Ni foam and Pt sheet for comparison. Production of alkaline-efficient electrocatalysts is of prime importance because alkaline water electrolysis is most widely used in the industry. The Co_xO_y/NF electrode is proven to have good HER performance in an alkaline solution. The LSV curves of Co_xO_y/NF in 1 M NaOH exhibit an overpotential of 80 mV at -10 mA/cm^2 (η_{10}) (Figure 5(a)), much smaller than those of the bare Ni foam (232 mV) and Pt sheet (114 mV). It indicates excellent HER activity for Co_xO_y/NF benefitting from its relatively larger surface area and more active sites exposed. Figure 5(b) shows the Tafel plots of the bare Ni foam, Co_xO_y/NF, and Pt sheet in 1 M NaOH. Tafel plots fit well with the Tafel equation: $\eta = b \times \log(j) + a$, where j is the current density and b is

Table 2: HER performances of Co-Pi/CoP, Co_xO_y, and other reported electrocatalysts (j: current density; η: overpotential).

Catalyst	Media	j (mA/cm^2)	η (mV)	Tafel slope (mV dec^{-1})	Ref.
Co_xO_y	1 M NaOH	10	80	110.1	This work
Co-Pi/CoP	0.5 M H_2SO_4	10	112	99.8	This work
Cobalt phosphide/phosphate thin film (PCPTF)	1 M KOH	30	430	—	[28]
	0.5 M H_2SO_4	30	175	53	
NiFeOx/CFP	1 M KOH	10	88	118	[41]
Co-P film	1 M KOH	10	94	120	[42]
Ni/NiP	1 M KOH	10	130	106	[43]
Ni_5P_4 films	1 M KOH	10	150	59	[44]
	0.5 M H_2SO_4	10	140	40	
Co_3O_4	1 M KOH	10	~260	—	[45]
$Ni(OH)_2$–CoS_2/CC	1 M KOH	20	99	118	[46]
$Co(OH)_2$@PANI HNSs/NF	1 M KOH	10	88	91.6	[37]
$Ni(OH)_2/MoS_2$@CC	1 M KOH	10	80	60	[47]
CoPt@$Co(OH)_2$	1 M KOH	10	~150	73	[48]
$Ni(OH)_2$–Fe_2P/TM	1 M KOH	10	76	105	[49]
CoS-$Co(OH)_2$@aMoS_{2+x}/NF	1 M KOH	10	140	68	[36]

the Tafel slope. The Tafel slopes of the three electrodes were calculated as 199.8, 110.1, and 104.2 mV/dec, respectively. Obviously, the bare Ni foam shows a higher slope than the Co_xO_y/NF electrode and Pt sheet, which is consistent with the HER activity evaluated with LSV curves. The Co_xO_y/NF electrode also shows superior activity to similar electrocatalysts reported (Table 2).

The good stability of the time dependence with the current density is also essential for the long-term application of electrocatalysts. Figure 5(c) demonstrates that the current density of the Co_xO_y/NF electrode in 1 M NaOH at an overpotential of 80 mV remains quite stable in a time range of 40,000 s, which can prove the excellent stability of the electrode. Figure 5(d) shows linear sweep voltammetry curves of Co_xO_y/NF before and after potential sweeps between −0.2 and +0.2 V vs. RHE for 3000 cycles. With almost no shifts between each curve, it further proves the long-term stability.

In contrast to the Co_xO_y/NF electrode, Figures 6(a)–6(d) exhibit the catalytic activity of the bare Ni foam, Co-Pi/CoP/NF electrode, and Pt sheet showing that the Co-Pi/CoP/NF electrode has a lower η_{10} of 112 mV than the bare Ni foam (over 300 mV), and just a little higher than that of the Pt sheet (84 mV) (Figure 6(a)). The Tafel slope of the Co-Pi/CoP/NF electrode (ca. 99.8 mV/dec) is lower than the bare Ni foam (ca. 282.3 mV/dec) and a little higher than that of the Pt sheet (ca. 37.3 mV/dec) (Figure 6(b)). It also ranks among the best of similar electrocatalysts reported (Table 2). At the same time, the time dependence of the current density test and polarization curves obtained over Co-Pi/CoP/NF before and after potential sweeps between −0.2 and +0.2 V vs. RHE (Figures 6(c)–6(d)) also proves the good stability of the Co-Pi/CoP/NF electrode, the same as the Co_xO_y/NF electrode.

Considering the excellent catalytic performance of Co-Pi/CoP and Co_xO_y for HER, the synergetic effect of Co (+2) and Co (+3) may play an important role during the process. The proposed mechanism is illustrated in Scheme 1. As reported by a previous study [37], the adsorption and desorption of the H atom are the key procedures for HER. Gibbs' free energy (ΔG_{H*}) of absorbed H atoms on catalysts can efficiently characterize how difficult the adsorption and desorption of the H atom are. Pt possesses a nearly zero ΔG_{H*}, and higher or lower ΔG_{H*} can increase the difficulty for the desorption or adsorption of the H atom [38]. CoP has a relatively strong bond with H, which means it can easily adsorb H but may suffer from the desorption of H [39, 40]. In contrast, Co-Pi has a weaker bond with H. The compounds of Co-Pi and CoP can enhance the adsorption and desorption at the same time. Through the synergy between Co-Pi and CoP, an outstanding catalytic activity is achieved. The synergetic effect of Co_xO_y along with Co (+2) and Co (+3) remains the same.

4. Conclusions

A Co-P precursor is successfully synthesized on Ni foam with a simple electrodeposition method. After being selectively treated in an alkaline or acidic solution, the obtained electrodes can be used for HER in an alkaline or acidic electrolyte. Both Co_xO_y/NF and Co-Pi/CoP/NF electrodes show excellent HER activity, comparable to the Pt sheet. The changed composition of the electrodes with the treating precursor in an acidic or alkaline solution is the main factor that leads to different catalytic characteristics. The synergy between Co (+2) and Co (+3) may also play an important role in the reaction. This work may give a new thinking to exploit new electrocatalysts for HER.

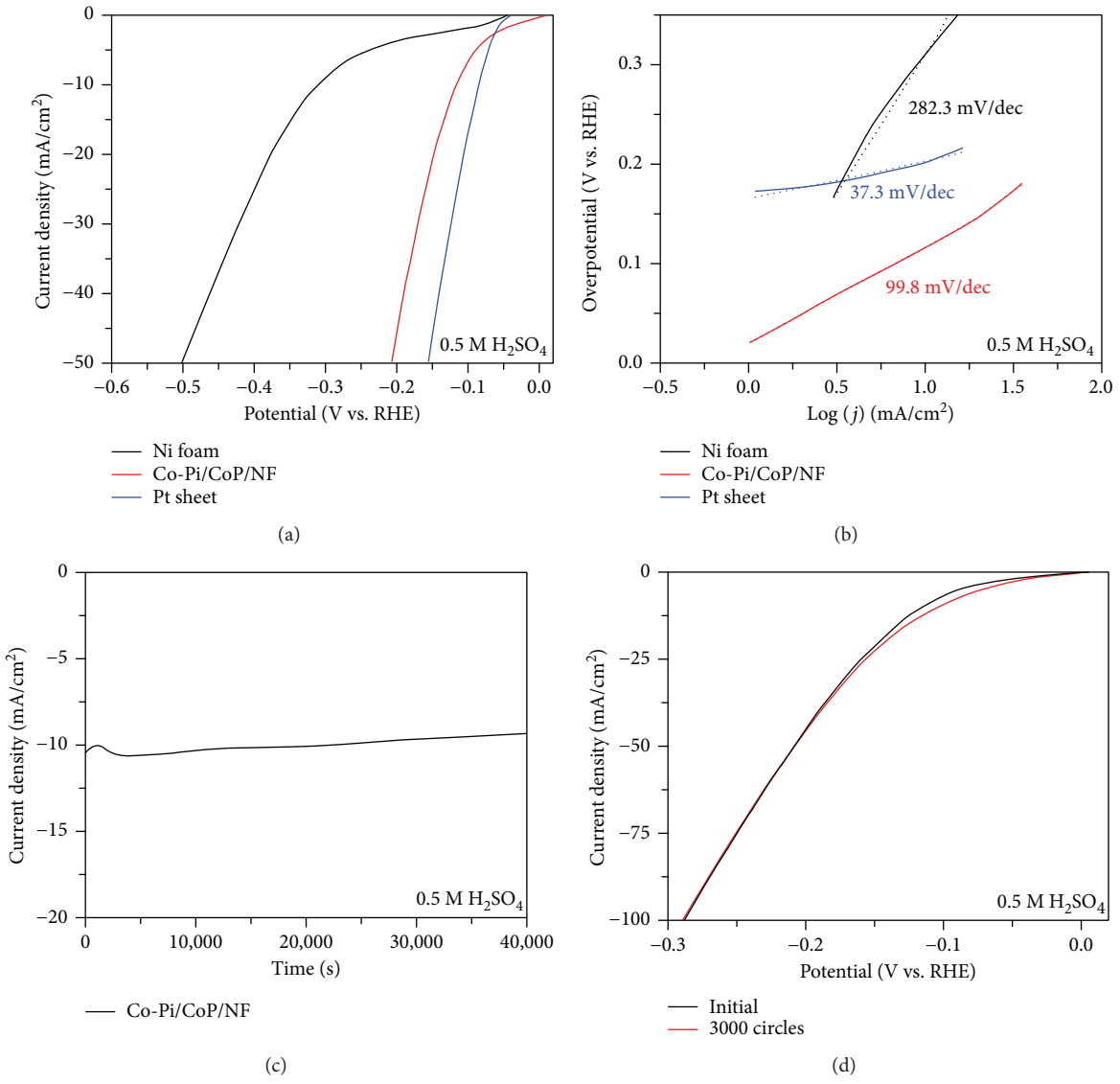

Figure 6: (a) LSV polarization curves for HER and (b) the corresponding Tafel slopes of bare Ni Foam, Co-Pi/CoP/NF, and Pt sheet in 0.5 M H_2SO_4 (pH = 0). (c) Chronoamperometry curves of the long-term stability of the Co-Pi/CoP/NF electrode at a static overpotential of 112 mV in 0.5 M H_2SO_4. (d) Polarization curves obtained over Co-Pi/CoP/NF before and after potential sweeps between −0.2 and +0.2 V vs. RHE for 3000 cycles with a scan rate of 0.1 V/s.

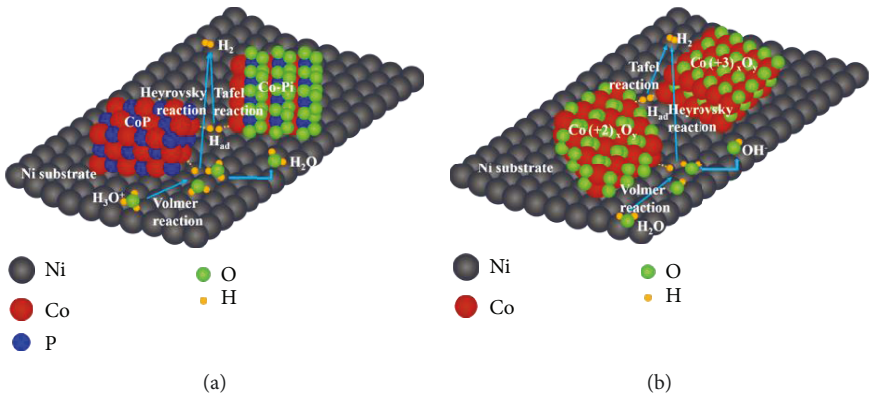

Scheme 1: Mechanism and the synergetic effect of (a) Co-Pi/CoP in acidic medium and (b) Co_xO_y in alkaline medium for HER.

Data Availability

The data used to support the findings of this study are available from the corresponding author upon request.

Conflicts of Interest

The authors declare that they have no conflicts of interest.

Acknowledgments

This work was supported by the 973 Programs (no. 2014CB239302), the National Natural Science Foundation of China (nos. 21473091 and 21773114), and the Applied Basic Research Programs of the Science & Technology Department of Sichuan Province (2017JY0146).

References

[1] J. A. Turner, "Sustainable hydrogen production," *Science*, vol. 305, no. 5686, pp. 972–974, 2004.

[2] G. W. Crabtree, M. S. Dresselhaus, and M. V. Buchanan, "The hydrogen economy," *Physics Today*, vol. 57, no. 12, pp. 39–44, 2004.

[3] D. G. Nocera, "The artificial leaf," *Accounts of Chemical Research*, vol. 45, no. 5, pp. 767–776, 2012.

[4] J. Greeley, T. F. Jaramillo, J. Bonde, I. Chorkendorff, and J. K. Nørskov, "Computational high-throughput screening of electrocatalytic materials for hydrogen evolution," *Nature Materials*, vol. 5, no. 11, pp. 909–913, 2006.

[5] T. R. Cook, D. K. Dogutan, S. Y. Reece, Y. Surendranath, T. S. Teets, and D. G. Nocera, "Solar energy supply and storage for the legacy and nonlegacy worlds," *Chemical Reviews*, vol. 110, no. 11, pp. 6474–6502, 2010.

[6] H. Dau, C. Limberg, T. Reier, M. Risch, S. Roggan, and P. Strasser, "The mechanism of water oxidation: from electrolysis via homogeneous to biological catalysis," *ChemCatChem*, vol. 2, no. 7, pp. 724–761, 2010.

[7] X. Zou and Y. Zhang, "Noble metal-free hydrogen evolution catalysts for water splitting," *Chemical Society Reviews*, vol. 44, no. 15, pp. 5148–5180, 2015.

[8] B. Liu, Y. F. Zhao, H. Q. Peng et al., "Nickel–cobalt diselenide 3D mesoporous nanosheet networks supported on Ni foam: an all-pH highly efficient integrated electrocatalyst for hydrogen evolution," *Advanced Materials*, vol. 29, no. 19, article 1606521, 2017.

[9] F. Safizadeh, E. Ghali, and G. Houlachi, "Electrocatalysis developments for hydrogen evolution reaction in alkaline solutions—a review," *International Journal of Hydrogen Energy*, vol. 40, no. 1, pp. 256–274, 2015.

[10] B. M. Jovic, V. D. Jovic, U. C. Lacnjevac, L. Gajic-krstajic, and N. V. Krstajic, "Ni-(Ebonex-supported Ir) composite coatings as electrocatalysts for alkaline water electrolysis. Part I: hydrogen evolution," *International Journal of Hydrogen Energy*, vol. 40, no. 33, pp. 10480–10490, 2015.

[11] H. Zhang, X. Li, A. Hähnel et al., "Bifunctional heterostructure assembly of NiFe LDH nanosheets on NiCoP nanowires for highly efficient and stable overall water splitting," *Advanced Functional Materials*, vol. 28, no. 14, article 1706847, 2018.

[12] Y. Li, H. Wang, L. Xie, Y. Liang, G. Hong, and H. Dai, "MoS_2 nanoparticles grown on graphene: an advanced catalyst for the hydrogen evolution reaction," *Journal of the American Chemical Society*, vol. 133, no. 19, pp. 7296–7299, 2011.

[13] J. O.'. M. Bockris and E. C. Potter, "The mechanism of the cathodic hydrogen evolution reaction," *Journal of the Electrochemical Society*, vol. 99, no. 4, pp. 169–186, 1952.

[14] L. Zhang, L. Han, H. Liu, X. Liu, and J. Luo, "Potential-cycling synthesis of single platinum atoms for efficient hydrogen evolution in neutral media," *Angewandte Chemie, International Edition*, vol. 56, no. 44, pp. 13694–13698, 2017.

[15] K. Xiong, L. Li, L. Zhang et al., "Ni-doped Mo_2C nanowires supported on Ni foam as a binder-free electrode for enhancing the hydrogen evolution performance," *Journal of Materials Chemistry A*, vol. 3, no. 5, pp. 1863–1867, 2015.

[16] L.-L. Feng, G. Yu, Y. Wu et al., "High-index faceted Ni_3S_2 nanosheet arrays as highly active and ultrastable electrocatalysts for water splitting," *Journal of the American Chemical Society*, vol. 137, no. 44, pp. 14023–14026, 2015.

[17] Y. Wu, Y. Liu, G. D. Li et al., "Efficient electrocatalysis of overall water splitting by ultrasmall $Ni_xCo_{3-x}S_4$ coupled Ni_3S_2 nanosheet arrays," *Nano Energy*, vol. 35, pp. 161–170, 2017.

[18] Y. Liu, T. G. Kelly, J. G. Chen, and W. E. Mustain, "Metal carbides as alternative electrocatalyst supports," *ACS Catalysis*, vol. 3, no. 6, pp. 1184–1194, 2013.

[19] M. Nagai, Y. Goto, O. Uchino, and S. Omi, "TPD and XRD studies of molybdenum nitride and its activity for hydrodenitrogenation of carbazole," *Catalysis Today*, vol. 43, no. 3-4, pp. 249–259, 1998.

[20] W.-F. Chen, K. Sasaki, C. Ma et al., "Hydrogen-evolution catalysts based on non-noble metal nickel-molybdenum nitride nanosheets," *Angewandte Chemie International Edition*, vol. 51, no. 25, pp. 6131–6135, 2012.

[21] Q. Liu, J. Tian, W. Cui et al., "Carbon nanotubes decorated with CoP nanocrystals: a highly active non-noble-metal nanohybrid electrocatalyst for hydrogen evolution," *Angewandte Chemie International Edition*, vol. 53, no. 26, pp. 6710–6714, 2014.

[22] P. Xiao, M. A. Sk, L. Thia et al., "Molybdenum phosphide as an efficient electrocatalyst for the hydrogen evolution reaction," *Energy & Environmental Science*, vol. 7, no. 8, pp. 2624–2629, 2014.

[23] J. Huang, J. Chen, T. Yao et al., "CoOOH nanosheets with high mass activity for water oxidation," *Angewandte Chemie International Edition*, vol. 127, no. 30, pp. 8846–8851, 2015.

[24] P. Guo, J. Wu, X. B. Li et al., "A highly stable bifunctional catalyst based on 3D $Co(OH)_2$@NCNTs@NF towards overall water-splitting," *Nano Energy*, vol. 47, pp. 96–104, 2018.

[25] S. H. Hong, S. H. Ahn, J. Choi et al., "High-activity electrodeposited NiW catalysts for hydrogen evolution in alkaline water electrolysis," *Applied Surface Science*, vol. 349, pp. 629–635, 2015.

[26] J. Tian, Q. Liu, A. M. Asiri, and X. Sun, "Self-supported nanoporous cobalt phosphide nanowire arrays: an efficient 3D hydrogen-evolving cathode over the wide range of pH 0–14," *Journal of the American Chemical Society*, vol. 136, no. 21, pp. 7587–7590, 2014.

[27] P. Jiang, Q. Liu, Y. Liang, J. Tian, A. M. Asiri, and X. Sun, "A cost-effective 3D hydrogen evolution cathode with high catalytic activity: FeP nanowire array as the active phase," *Angewandte Chemie International Edition*, vol. 53, no. 47, pp. 12855–12859, 2014.

[28] Y. Yang, H. Fei, G. Ruan, and J. M. Tour, "Porous cobalt-based thin film as a bifunctional catalyst for hydrogen generation and oxygen generation," *Advanced Materials*, vol. 27, no. 20, pp. 3175–3180, 2015.

[29] R. Zhang, X. Wang, S. Yu et al., "Ternary $NiCo_2P_x$ nanowires as pH-universal electrocatalysts for highly efficient hydrogen evolution reaction," *Advanced Materials*, vol. 29, no. 9, article 1605502, 2017.

[30] L. Xie, R. Zhang, L. Cui et al., "High-performance electrolytic oxygen evolution in neutral media catalyzed by a cobalt phosphate nanoarray," *Angewandte Chemie International Edition*, vol. 56, no. 4, pp. 1064–1068, 2017.

[31] L. Ai, Z. Niu, and J. Jiang, "Mechanistic insight into oxygen evolution electrocatalysis of surface phosphate modified cobalt phosphide nanorod bundles and their superior performance for overall water splitting," *Electrochimica Acta*, vol. 242, pp. 355–363, 2017.

[32] Y. Xin, X. Kan, L. Y. Gan, and Z. Zhang, "Heterogeneous bimetallic phosphide/sulfide nanocomposite for efficient solar-energy-driven overall water splitting," *ACS Nano*, vol. 11, no. 10, pp. 10303–10312, 2017.

[33] P. Arunachalam, M. Shaddad, A. Alamoudi, M. Ghanem, and A. al-Mayouf, "Microwave-assisted synthesis of $Co_3(PO_4)_2$ nanospheres for electrocatalytic oxidation of methanol in alkaline media," *Catalysts*, vol. 7, no. 12, 2017.

[34] A. Samal, S. Swain, B. Satpati, D. P. Das, and B. K. Mishra, "3 D $Co_3(PO_4)_2$-reduced graphene oxide flowers for photocatalytic water splitting: a type II staggered heterojunction system," *ChemSusChem*, vol. 9, no. 22, pp. 3150–3160, 2016.

[35] Q. Zhou, T. T. Li, J. Qian, Y. Hu, F. Guo, and Y. Q. Zheng, "Self-supported hierarchical CuO_x@Co_3O_4 heterostructures as efficient bifunctional electrocatalysts for water splitting," *Journal of Materials Chemistry A*, vol. 6, no. 29, pp. 14431–14439, 2018.

[36] T. Yoon and K. S. Kim, "One-step synthesis of CoS-doped β-Co(OH)2@amorphous MoS_{2+x} hybrid catalyst grown on nickel foam for high-performance electrochemical overall water splitting," *Advanced Functional Materials*, vol. 26, no. 41, pp. 7386–7393, 2016.

[37] J. X. Feng, L. X. Ding, S. H. Ye et al., "$Co(OH)_2$@PANI hybrid nanosheets with 3D networks as high-performance electrocatalysts for hydrogen evolution reaction," *Advanced Materials*, vol. 27, no. 44, pp. 7051–7057, 2015.

[38] Q. Lu, Y. Yu, Q. Ma, B. Chen, and H. Zhang, "2D transition-metal-dichalcogenide-nanosheet-based composites for photocatalytic and electrocatalytic hydrogen evolution reactions," *Advanced Materials*, vol. 28, no. 10, pp. 1917–1933, 2016.

[39] D.-H. Ha, B. Han, M. Risch et al., "Activity and stability of cobalt phosphides for hydrogen evolution upon water splitting," *Nano Energy*, vol. 29, pp. 37–45, 2016.

[40] J. Kibsgaard, C. Tsai, K. Chan et al., "Designing an improved transition metal phosphide catalyst for hydrogen evolution using experimental and theoretical trends," *Energy & Environmental Science*, vol. 8, no. 10, pp. 3022–3029, 2015.

[41] H. Wang, H. W. Lee, Y. Deng et al., "Bifunctional non-noble metal oxide nanoparticle electrocatalysts through lithium-induced conversion for overall water splitting," *Nature Communications*, vol. 6, no. 1, pp. 7261–7268, 2015.

[42] N. Jiang, B. You, M. Sheng, and Y. Sun, "Electrodeposited cobalt-phosphorous-derived films as competent bifunctional catalysts for overall water splitting," *Angewandte Chemie International Edition*, vol. 54, no. 21, pp. 6251–6254, 2015.

[43] G. F. Chen, T. Y. Ma, Z. Q. Liu et al., "Efficient and stable bifunctional electrocatalysts Ni/Ni_xM_y (M = P, S) for overall water splitting," *Advanced Functional Materials*, vol. 26, no. 19, pp. 3314–3323, 2016.

[44] M. Ledendecker, S. Krick Calderón, C. Papp, H. P. Steinrück, M. Antonietti, and M. Shalom, "The synthesis of nanostructured Ni5 P4 films and their use as a non-noble bifunctional electrocatalyst for full water splitting," *Angewandte Chemie, International Edition*, vol. 54, no. 42, pp. 12361–12365, 2015.

[45] G. Cheng, T. Kou, J. Zhang, C. Si, H. Gao, and Z. Zhang, "O_2^{2-}/O^- functionalized oxygen-deficient Co_3O_4 nanorods as high performance supercapacitor electrodes and electrocatalysts towards water splitting," *Nano Energy*, vol. 38, pp. 155–166, 2017.

[46] L. Chen, J. Zhang, X. Ren et al., "A $Ni(OH)_2$–CoS_2 hybrid nanowire array: a superior non-noble-metal catalyst toward the hydrogen evolution reaction in alkaline media," *Nanoscale*, vol. 9, no. 43, pp. 16632–16637, 2017.

[47] B. Zhang, J. Liu, J. Wang et al., "Interface engineering: the $Ni(OH)_2/MoS_2$ heterostructure for highly efficient alkaline hydrogen evolution," *Nano Energy*, vol. 37, pp. 74–80, 2017.

[48] B. Malik, S. Anantharaj, K. Karthick, D. K. Pattanayak, and S. Kundu, "Magnetic CoPt nanoparticle-decorated ultrathin $Co(OH)_2$ nanosheets: an efficient bi-functional water splitting catalyst," *Catalysis Science & Technology*, vol. 7, no. 12, pp. 2486–2497, 2017.

[49] X. Zhang, S. Zhu, L. Xia, C. Si, F. Qu, and F. Qu, "$Ni(OH)_2$–Fe_2P hybrid nanoarray for alkaline hydrogen evolution reaction with superior activity," *Chemical Communications*, vol. 54, no. 10, pp. 1201–1204, 2018.